Geomechanics and Engineering, *Vol. 34, No. 2 (2023) 125-138*
https://doi.org/10.12989/gae.2023.34.2.125

Infiltration characteristic of modified slurry and support efficiency of filter cake in silty sand strata

Sai Zhang[a], Jianwen Ding*, Ning Jiao, Shuai Sun and Jinyu Liu

Department of Underground Engineering, Southeast University,
NO.2 Southeast University Road, Jiangning District, Nanjing, China

(*Received August 8, 2022, Revised April 3, 2023, Accepted April 18, 2023*)

Abstract. To improve the understanding of infiltration characteristic of modified slurry and the support efficiency of filter cake in silty sand strata, the slurry infiltration (SI) and filter cake formation (FCF) were investigated in a laboratory apparatus. The water discharge and the excess pore pressure at different depths of silty sand strata were measured during SI. The relationship between permeability coefficient/thickness ratio of filter cake ($k_c/\Delta L$) and effective slurry pressure conversion rate of filter cake (η) were analyzed. Moreover, the SI and FCF process as well as the modification mechanism of CMC (carboxymethyl cellulose) were clarified. The experimental results indicate the formation of only external filter cake in the silty sand strata. The slurry particles obtain thicker water membrane after being modified by CMC, which blocks partial water path in filter cake and decreases the water discharge significantly. The silty sand excavated from tunnel face also contributes to the water discharge reduction. The k_c of the external filter cake ranges from 3.83×10^{-8} cm/s to 7.44×10^{-8} cm/s. The η of the external filter cake is over 96%, which decreases with increasing $k_c/\Delta L$. A silty sand content within 10% is suggested during construction to ensure the uniformity of the filter cake.

Keywords: filter cake formation; modified slurry; river-crossing tunnel; slurry infiltration; stability of tunnel face

1. Introduction

With rapid development of the Yangtze River Economic Belt in China, the construction of river-crossing tunnel is becoming more and more popular, which leads to a wider application of slurry shield (Lin *et al.* 2013). Many project practices (e.g., Xiamen Line 2, Line 3 tunnels, Yangtze River tunnel) have demonstrated the efficiency of slurry shield in underwater tunnel construction (Min *et al.* 2015, Min *et al.* 2018). However, some problems are commonly encountered during slurry shield, such as cutterhead abrasion, blocking in cutter carrier, etc. (Zhao *et al.* 2007). Consequently, the chamber opening is required to create a working space for the cutterhead inspection and maintenance (Li and Yuan 2018). As acknowledged, the chamber opening can be conducted under the atmospheric pressure condition in an initially stable or pre-reinforced strata. On the contrary, it must be conducted under the support of compressed air pressure by forming a filter cake (Aydina *et al.* 2004).

FCF is a classic solid-liquid separation process (Ni *et al.* 2006), during which a micro-permeable filter cake is formed to transfer slurry pressure to balance the earth pressure and water pressure of strata during slurry shield (Zizka *et al.* 2021). In previous studies, infiltration column test (ICT) has been widely used to evaluate SI and FCF behavior. It is shown that a filter cake consisted of infiltration zone (mud spurt) and external filter cake could be formed provided adequate slurry pressure and time (Fritz *et al.* 2002, Zizka *et al.* 2018).

The mud spurt has been proved to improve the cohesion of the strata and prevent the failure of excavation face to some extent (Hu and Zhang 2009). However, in some cohesionless soil strata where slurry can hardly infiltrate, the only way to maintain the stability of excavation face is to prevent a seepage flow towards the excavation face (Anagnostou and Kovári 1994). Thus, in some cases, the slurry needs to be modified to enhance the impermeability of the filter cake. Many previous researches have presented that the modification materials (CMC (carboxymethyl cellulose), XG (xanthan gum), etc.) play significant roles in slurry modification (Min *et al.* 2019, Wei *et al.* 2020, Mao *et al.* 2021).

Meanwhile, the slurry in the work chamber is often combined with the excavated soil during shield tunneling. It is seldom considered in previous researches, which may also lead to the variation of filter cake property (Xu and Bezuijen 2018). Furthermore, the support efficiency is rarely discussed with respect to the varied excavated soil content.

To investigate the CMC modified slurry mixed with excavated soil and the support efficiency of filter cake, a series of ICTs were conducted based on a river-crossing tunnel constructed in silty sand in Nanjing, China. The infiltration characteristics of slurry containing CMC and silty sand were investigated. The water discharge and the excess pore pressure were measured during ICTs. The relationship between $k_c/\Delta L$ and the η was proposed. Moreover, the SI and FCF process as well as the modification mechanism of CMC were explained. The study may provide references for slurry shield construction of river-crossing tunnel in silty sand strata.

*Corresponding author, Professor
E-mail: jwding@seu.edu.cn
[a]Ph.D. Student
E-mail: zhangsai@seu.edu.cn

ISSN: 2005-307X (Print), 2092-6219 (Online)

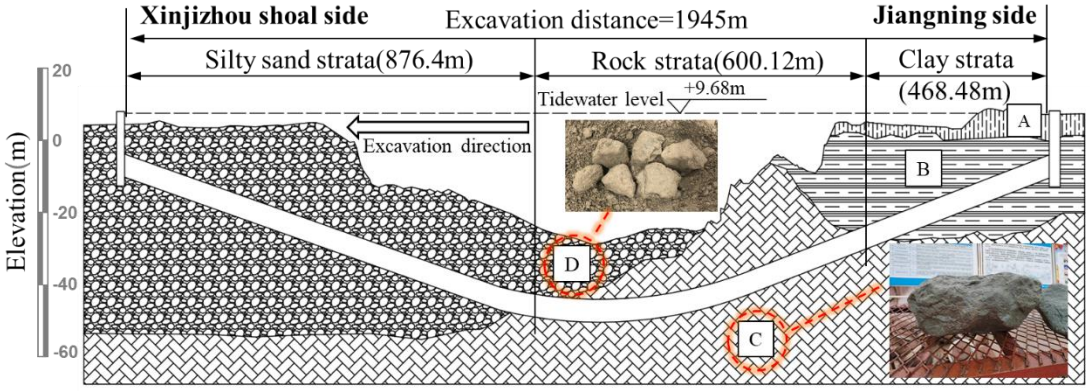

Fig. 1 Soil profile and location of tunnel. A: Silt and silty clay, B: Muddy silty clay, C: Medium weathered diorite porphyrite, D: Silty sand

2. Project overview

2.1 Project information

Xinjizhou shoal water supply project locates in the lower reaches of Yangtze River, which is bulit to supply water in Jiangning district of Nanjing, China. The project is composed of water storage project, water transfer project, water supply corridor project and sewage treatment project. Slurry shield is used in the water supply corridor project, which consists of originating shaft, river-crossing tunnel and receiving shaft. The main geological strata of the tunnel section is plotted in Fig. 1.

The shield machine crosses through the Yangtze River from the originating shaft on Jiangning side to the receiving shaft on Xinjizhou shoal side. The shield interval has a total length of 1945 m, including 468.5 m of clay strata, 600.1 m of rock strata and 876.5 m of sand strata. The longitudinal section of the river-crossing tunnel is a V-shaped slope with the maximum slope (ratio) of 45.85‰. The outer diameter and the inner diameter of the tunnel are 6.2 m and 5.5 m, respectively. The tidewater level is 9.68 m, the buried depth of tunnel is 8~51.5 m, and the highest water pressure of tunnel is 0.52 MPa.

2.2 Construction problems

It should be noted that the medium weathered diorite porphyrite strata easily causes the abrasion of cutters, where the chamber opening is required to create a working space for the cutterhead inspection and maintenance. In terms of the rock strata with low permeability and high strength, the chamber opening can be conducted just under atmospheric pressure condition. By contrast, when the machine passes through the silty sand strata, hard quartz and rock may also lead to the abrasion of cutters. Considering the high permeability (k_c=3×10^{-3} cm/s) and the high water pressure (0.52 MPa) of the silty sand strata, the chamber opening must be conducted under compressed air pressure (Li and Yuan 2018). At the same time, it is easy for slurry to filter out in the strata concerning the strata with complex hydrogeological conditions and high permeability at the bottom of the river, which may lead to the failure of FCF. Accordingly, the effective support pressure and the stability of the excavation face will decrease significantly. Therefore, the security of chamber opening need to be considered particularly in sand strata.

3. Experimental study

3.1 Test apparatus

A test apparatus is designed to investigate the formation and the support efficiency of filter cake (Fritz 2007, Duong *et al.* 2013, Min *et al.* 2013), whose schematic layout is shown in Fig. 2. The test apparatus consists of a water supply set-up, an infiltration column with an inner diameter of 15 cm, an air pressure control and monitoring set-up, a leachate collection set-up, an air compressor and a pore pressure monitoring system. The infiltration column is the core component of the apparatus, which consists of a plexiglass column, three water stoppers, a flange, five pressure transducers and a calibration sticker. The pore pressure transducers (K1~K5 from top to bottom) are installed isometrically (10cm) on the wall of plexiglass column to measure the pore pressure in different depths of strata during ICT (Zhang *et al*. 2017).

3.2 Materials

The amount of different materials was determined based on the weight of the water. The pure slurry with a constant Na-bentonite/water ratio of 8% had been hydrated for 24 hours before the tests. Then, different types of bentonite slurries with various silty sand content and CMC content were prepared.

The grain size distributions of silty sand and Na-bentonite used in the experiment were tested by sieves and hydrometer according to ASTM D422-63. Among them, the distribution of particle sizes larger than 75 μm and smaller than 75 μm is determined by sieving and hydrometer, respectively. The results are plotted in Fig. 3. It can be seen that the particle size of Na-bentonite is much smaller than silty sand, which makes it possible for Na-bentonite to infiltrate into the strata and clog the pores.

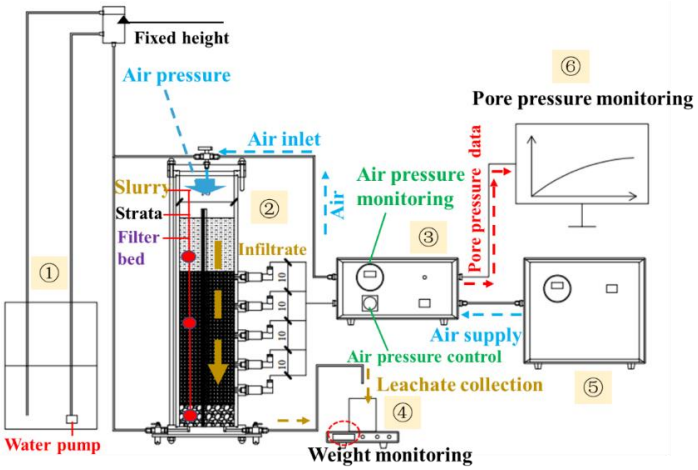

Fig. 2 Schematic layout of test apparatus: ①: Water supply set-up, ②: Infiltration column, ③: Air pressure control and monitoring set-up, ④: Leachate collection set-up, ⑤: Air compressor, ⑥: Pore pressure monitoring system

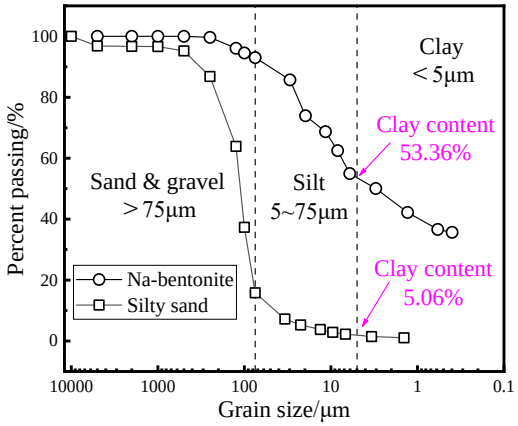

Fig. 3 Grain size distributions of tested soils

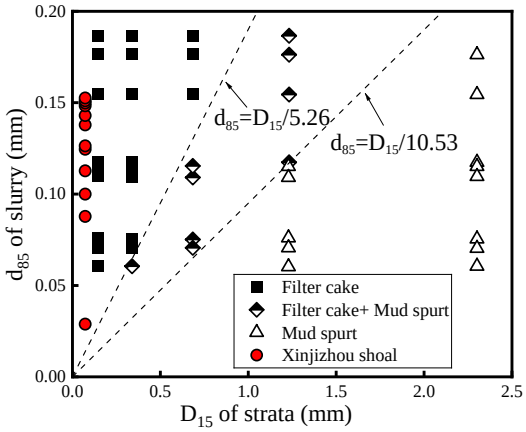

Fig. 4 Relationship between slurry particle and strata soil

Min *et al*. (2013) proposed three types of filter cake through a series of ICTs (see Fig. 4). Based on this, the characteristic size of strata (D_{15}- particle size for which 15% by weight of particles in the strata are smaller) and slurry particle (d_{85}-particle size for which 85% by weight of particles in the slurry are smaller) were chosen to establish the judgment basis of filter cake types. In this investigation, the D_{15} of strata soil is 0.0723 mm, the d_{85} of 12 types of bentonite slurries with 0%~34% silty sand content are listed in Table 1.

To judge the type of filter cake forms in Xinjizhou shoal strata, the relationship between slurry particle and strata soil is illustrated in Fig. 4. As shown in the figure, the points of Xinjizhou shoal strata are all distributed in the upper left of

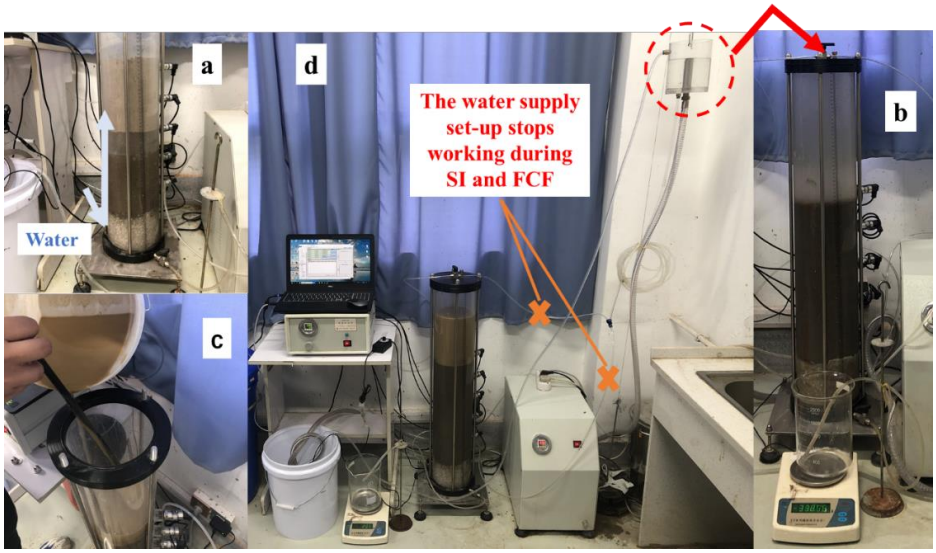

Fig. 5 Major procedures of ICT: (a): Strata saturation, (b): Hydraulic conductivity test, (c): Slurry addition and (d): SI and FCF

Table 1 The characteristic size of slurry particles

Silty sand content (%)	d_{85} (mm)	Silty sand content (%)	d_{85} (mm)	Silty sand content (%)	d_{85} (mm)
0	0.029	8	0.125	22	0.148
2	0.878	10	0.126	26	0.150
4	0.100	14	0.138	30	0.151
6	0.113	18	0.143	34	0.153

Table 2 The physical properties of slurries

	Silty sand content (%)	CMC content (‰)	Density (g/cm^3)	Funnel viscosity (s)
S0C0	0	0	1.04	35
S0C1	0	1	1.04	40
S0C2	0	2	1.04	45
S0C3	0	3	1.04	51
S2C0	2	0	1.05	34
S2C2	2	2	1.05	45
S4C2	4	2	1.06	47
S6C1	6	1	1.08	42
S8C1	8	1	1.09	40
S10C1	10	1	1.11	43

the straight line $d_{85} = D_{15} / 5.26$. It can be deduced that only the external filter cake is formed by the slurry in Xinjizhou shoal strata.

3.3 Experimental procedures

Fig. 5 presents the major procedures of ICT. Firstly, the filter bed with a 11~12 cm layer of gravel, as well as the strata with a 45 cm layer of silty sand were prepared. During the strata preparation, the total weight of the required dry silty sand was calculated based on the dry density of the in-situ silty sand in Xinjizhou shoal (ρ_d = 1.53g/cm^3). Then it is divided into 9 equal parts. After that, every part of dry silty sand was poured into the column from a fixed drop height (about 50cm) to ensure the uniformity of the strata. Note that the strata was gently compacted with plastic plate after each filling to ensure a 5cm rise of strata height. Then a fixed height of water was kept flowing into the strata from the bottom of the column to saturate the strata (see Fig. 5(a)). The hydraulic conductivity of the strata was determined to be 10^{-3} cm/s~10^{-2} cm/s according to ASTM D2434-06 (see Fig. 5(b)). The slurry was slowly injected along the inner wall of the infiltration column after the hydraulic conductivity test (see Fig. 5(c)). The final layer height of slurry was controlled to be approximately 20 cm. The slurry level, the upper surface height of the strata and the height of the gravel layer were read through the calibration sticker on the column wall. The initial pore pressures from top to bottom were recorded, respectively.

The flange was closed and the device was sealed before SI. Then, the compressed air pressure controlled by air pressure control and monitoring set-up was conducted on the slurry. At the same time, the infiltration type of the slurry was observed through the infiltration column, the pore pressure was recorded by pore pressure monitoring system, and the leachate was measured by an electronic scale (see Fig. 5(d)). The experiment was stopped either the leachate turned turbid or the water discharge increased rapidly, which means a large quantity of SI and the failure of FCF. The filter cake and part of the strata were taken out by a ring knife after the ICT, and the thickness of the external filter cake and the depth of the infiltration zone were measured. Finally, the water content of filter cake was determined by oven-drying method.

The loading air pressure of each stage was 50 kPa, after infiltrating for 5 minutes when the weight of water discharge variation less than 1.5 g per 10 seconds during the test, 50 kPa higher air pressure will be applied until

Fig. 6 Formation of filter cake

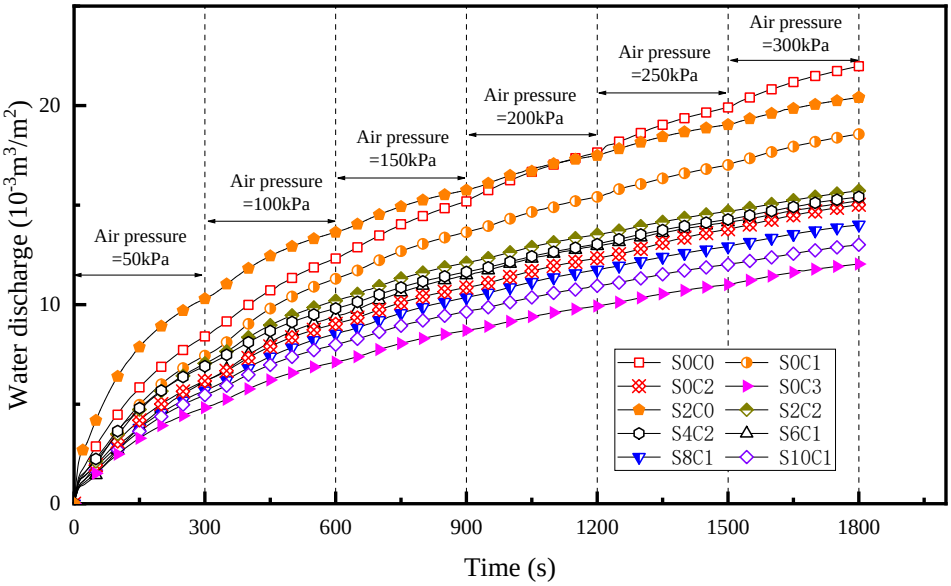

Fig. 7 SI curve of tested slurries

reaching a pressure of 300 kPa. A detailed description of the loading method can be found elsewhere (Min *et al*. 2013). Ten types of slurry with different CMC content and silty sand content were selected for ICTs, whose physical properties are summarized in Table 2.

According to the results, appropriate types of slurry, air pressure and infiltration time were selected for further ICTs to verify the support efficiency of filter cake, which will be discussed in section 4.2.

4. Results

4.1 SI and FCF behavior

Fig. 6 interprets the filter cake forms during the ICT. It is noticed that the slurry forms only external filter cake in Xinjizhou shoal strata, which is consistent with the judgement. Meanwhile, the lower part of filter cake is denser than the upper part, which can be explained from two aspects as follows: on the one hand, the lower part of filter cake is forms earlier and is compressed for longer time; on the other hand, the effective stress is larger for the lower part, leading to the lower part of filter cake be compressed more adequately than the upper part during the process of SI and FCF.

The SI curve of tested slurries is shown in Fig. 7. It can be seen that the variation rate of SI curve decreases with the increasing infiltration time under each level of loading. Meanwhile, it does not show a significant increase under the higher level of pressure, which reflects the good impermeability of the filter cake. As a result, the SI curve of all the measured slurries reaches a stable growth trend at the pressure of 300 kPa. Furthermore, the leachate was found clear throughout the ICTs, indicating that the strata can withstand 300 kPa of slurry pressure.

As depicted in Fig. 8, with the passage of SI under single-stage loading (50 kPa), the water discharge increases

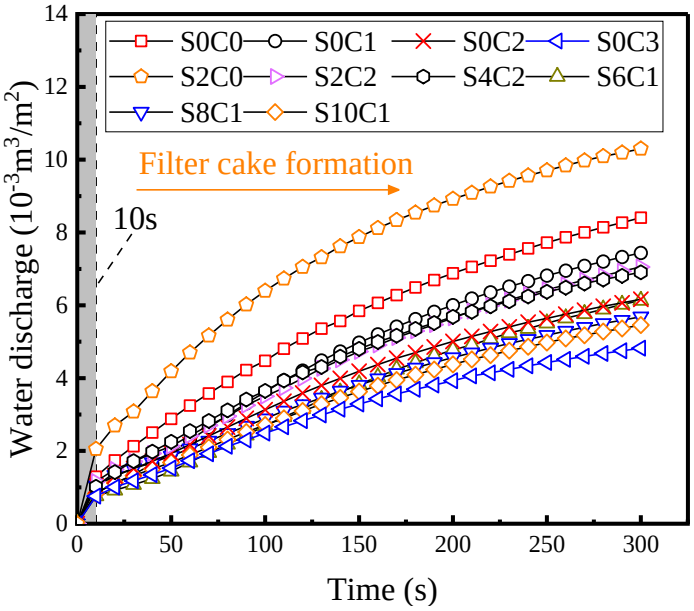

Fig. 8 SI curve of tested slurries under the first single-stage loading

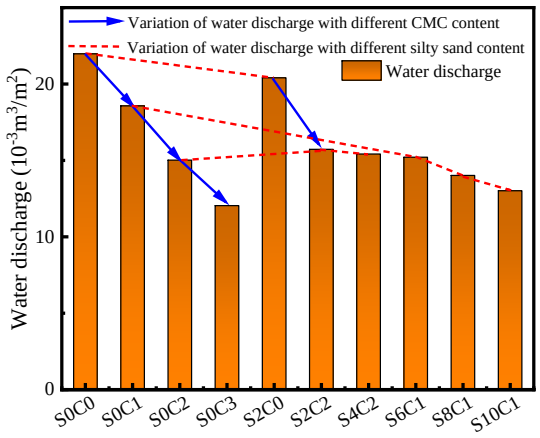

Fig. 9 Total water discharge of slurries

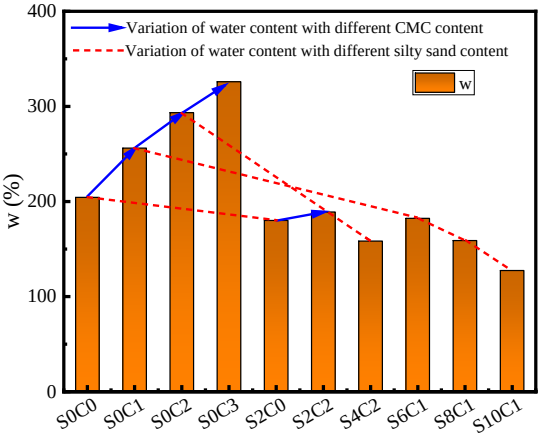

Fig. 10 Water content of filter cake

fastest during the first 10 seconds, which accounts for about one-fifth of the total water discharge in the first five minutes. indicating the formation and the permeability reduction of filter cake. As a result, it can be considered that the micro-permeable filter cake is formed directly at the beginning of the tests (Talmon *et al.* 2013).

The total water discharge of slurries is illustrated in Fig. 9. Slurries S0C0 (pure slurry), S2C0 and S0C1, which have the lowest CMC content or silty sand content, obtain higher water discharges (21.98×10^{-3} m^3/m^2, 20.41×10^{-3} m^3/m^2, 18.57×10^{-3} m^3/m^2, respectively) than that of the other slurries. The water discharge decreases with increasing silty sand content, which can be inferred that the silty sand excavated from the tunnel face which deposit first to form primary external filter cake on the tunnel face during SI, which is beneficial to prevent the slurry infiltration. Meanwhile, note that the water discharge can be reduced by 15% obviously with only one thousandth of a percent increment of the CMC, which is 7.5~18.5 times the ratio of silty sand. One may infer that the CMC content has more significant influence on the water discharge than the silty sand content.

It can be observed in Fig. 10 that the water content of filter cake increases with the increasing CMC content but decreases with the increasing silty sand content. The water content of S0C3 is beyond 300%, which exceeds 1.5 times that of the S0C0. Although the increase in CMC content results in a significant increase in water content, which may cause the pore ratio decrease of the saturated filter cake, the water discharge of the filter cake still decreases obviously. This phenomenon further demonstrates the good contribution of CMC to water discharge reduction.

4.2 Permeability coefficient of filter cake

A series of tests were conducted to evaluate the permeability coefficient of filter cake. According to ICTs, the slurries S0C0, S2C0 and S0C1 with the highest water discharge in section 4.1 were excluded, the remaining types of slurry as well as the newly prepared slurry S14C1 were used. 100 kPa of air pressure was applied in the tests

Table 3 Thickness of filter cakes

	S0C2	S0C3	S2C2	S4C2	S6C1	S8C1	S10C1	S14C1
Thickness/cm	1.12	1.01	1.33	1.22	1.40	1.48	1.49	1.52

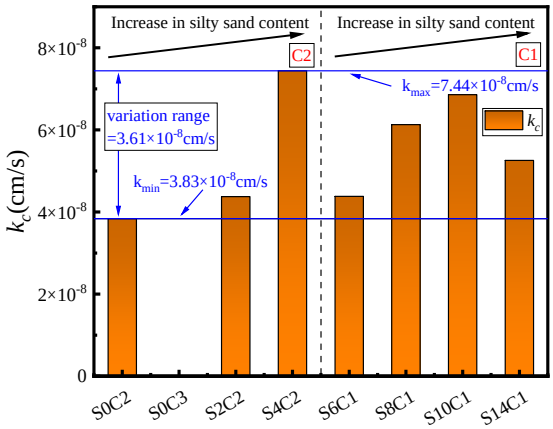

Fig. 11 Permeability coefficient of filter cakes

referring to Min *et al*. (2015). The tests lasted for 4 hours, the thicknesses and water content of filter cakes were measured after ICTs.

The thickness of filter cakes after FCF is summarized in Table 3. It can be seen that the thickness of filter cake increases with increasing silty sand content.

As reported by Xu and Bezuijen (2019), the influence of the strata can be neglected if its permeability is much higher (at least three orders of magnitude) than that of the filter cake. Considering the k_c of the strata is about 3×10^{-3} cm/s, and the k_c of the filter cake is of the order of 10^{-9}~10^{-6}cm/s (Xu and Bezuijen 2019, Min *et al*. 2019), the k_c of filter cake can be calculated following Darcy's law which shows in Eq. (1)

$$k_c = \frac{\Delta L Q}{\Delta h A} \tag{1}$$

Where ΔL denotes the thickness of filter cake; Q denotes the water discharge; Δh denotes the hydrostatic head between K1 and filter cake upper face; A denotes the cross-sectional area of the column.

Except for the k_c of filter cake S0C3, which is failed to be calculated since that the strata surface was compressed below the pore pressure transducer K1 during ICT, the k_c of other filter cakes is marked Fig. 11. It can be seen that the k_c ranges from 3.83×10^{-8} cm/s to 7.44×10^{-8} cm/s, which is coincident with Min *et al.* (2019). An increasing trend of k_c can be observed with increasing sand content. Moreover, the uniformity of the filter cake reduces with the increasing silty sand content (see Fig. 12). Particularly, an obvious sag appeared on the filter cake which was formed by S14C1. It can be deduced that the slurry mixed with silty sand of tunnel face during excavation not only increases the permeability of filter cake, but also worsened the uniformity of the filter cake. To avoid the potential threat of excavation tunnel face, the silty sand content is suggested to be within 10%.

4.3 Excess pore pressure distribution

The slurry pressure, a kind of pore pressure, is transformed into effective pressure to balance earth pressure by filter cake during FCF. Therefore, monitoring the soil excess pore pressure distribution is of great significance for analyzing the stability of tunnel excavation surface (Broere 2016, Park 2022, Zou *et al.* 2020). Previous researches (Bezuijen *et al*. 2006, Zizka and Thewes 2016) have shown that the SI in saturated strata will induce excess pore pressure, and the effective slurry pressure is transferred gradually rather than be transferred directly. The variation of excess pore pressure are plotted with respect to the square root of time, as illustrated in Fig. 13.

At the beginning of SI, the slurry cake is still too thin to prevent the seepage of water, the generation of the excess pore pressure caused by water penetration is faster than the dissipation of the excess pore pressure. The excess pore pressure approaches 50%~80% of slurry pressure subsequently, then 20-50% is effective stress. According to Lee *et al*. (2003), the support on excavation face majorly comes from effective pressure and seepage pressure (body force), the average seepage pressure is about 20%~30% of the pore pressure at the same elevation. Hence, the support on excavation face is too low to guarantee the tunnel stability. After around 5~15 $s^{-1/2}$, with the formation of the primary external filter cake at the boundary between the slurry and the strata, the excess pore pressure reduced significantly from K5 to K1 in order. The excess pore pressure dissipated first at the far end of the excavation face, indicating the reduction of the range influenced by seepage pressure. In this stage, with the formation of filter cake, the head loss in filter cake increases accordingly, contributing to the decrease of water seeping speed and the increase of effective slurry pressure. After about 20~40 $s^{-1/2}$, the curves reach an inflection point where a stable variation tendency of excess pore pressure appears.

(a) S2C2 (b) S10C1 (c) S14C1

Fig. 12 Filter cakes formed by different slurries

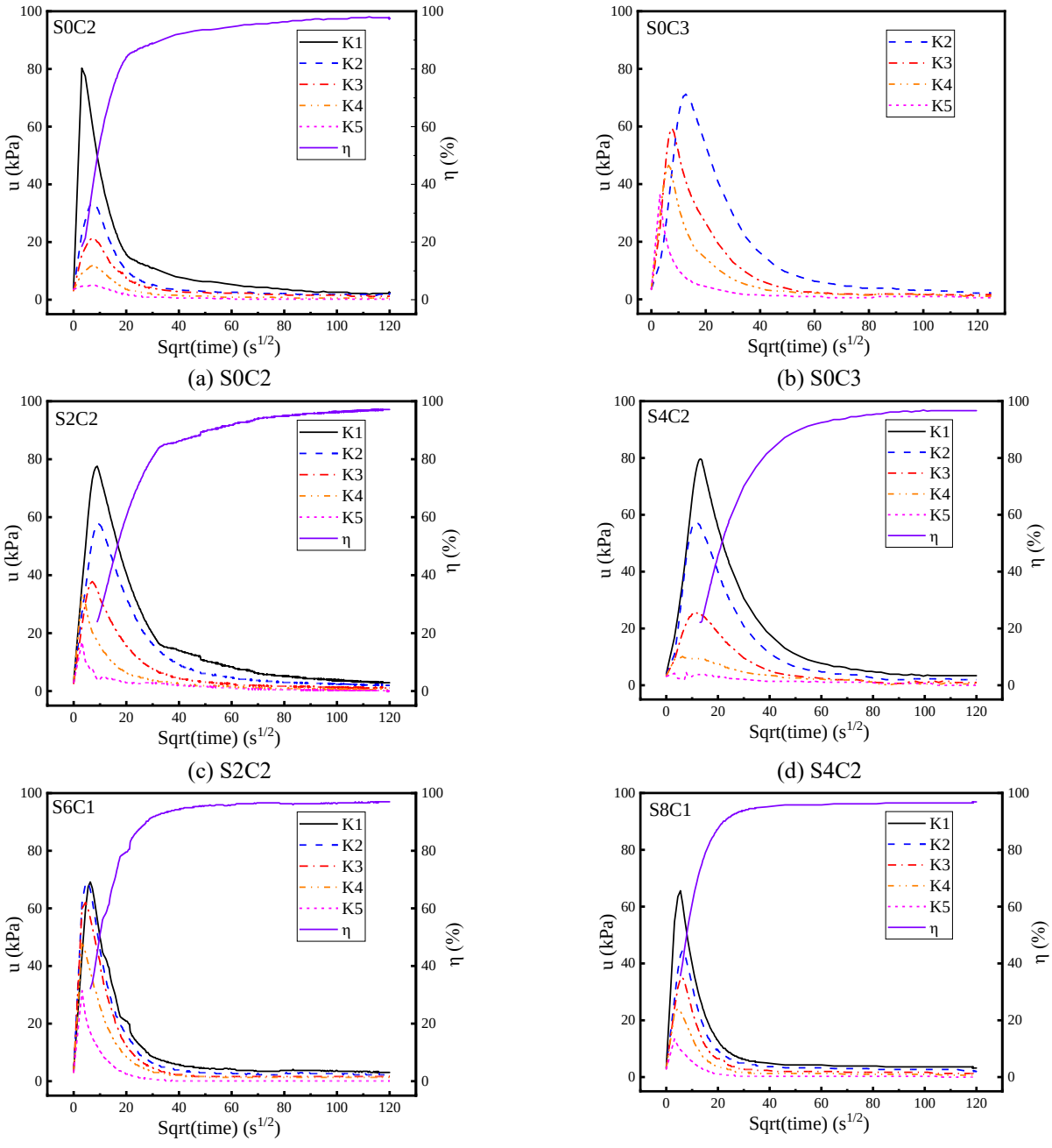

(a) S0C2 (b) S0C3

(c) S2C2 (d) S4C2

(e) S6C1 (f) S8C1

Fig. 13 Variations of excess pore pressure and effective slurry pressure conversion rate with time

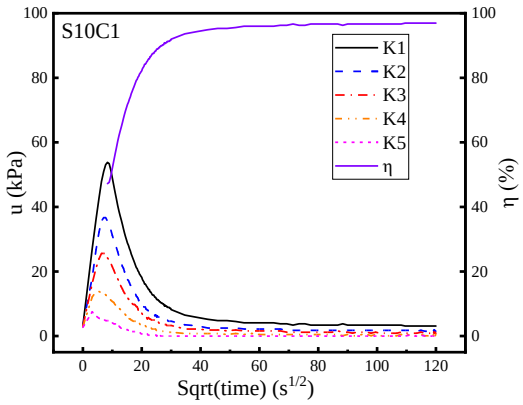

(g) S10C1

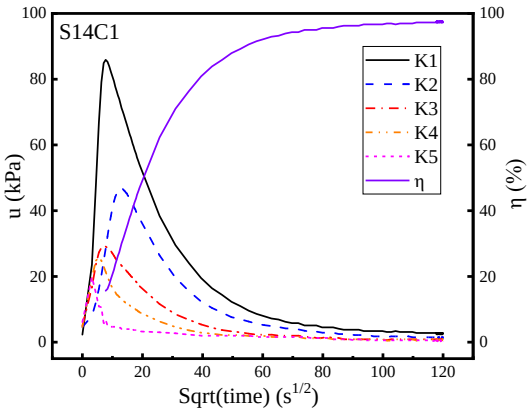

(h) S14C1

Fig. 13 Continued-

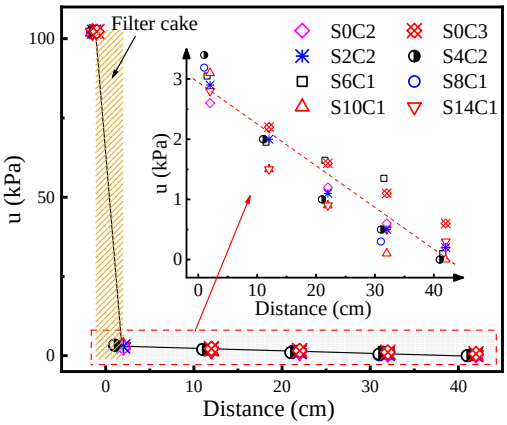

Fig. 14 Distribution of excess pore pressure in strata

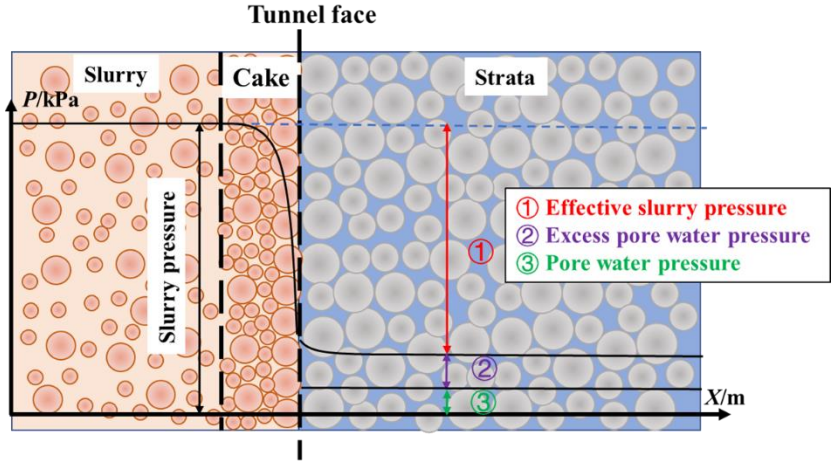

Fig. 15 Schematic layout of pressure distribution

Fig. 14 reflects the distribution of excess pore pressure in the strata after the steady of SI. It is seen that the variations of excess pore pressures are generally similar along depth. The hydraulic conductivity of the external filter cake is obviously lower than that in the strata, resulting in a dramatical hydraulic head decrease within the filter cake range. An effective slurry pressure increases significantly to support the tunnel face, the excess pore pressure decreases progressively and approaches a stable level with the increasing distance, which is consistent with Broere (2001). One may notice that the stable value of excess pore water pressure at the excavation surface is about 3 kPa, indicating that more than 96% of slurry pressure was transferred to the soil skeleton. The pressure distribution can be described more clearly by a microscale schematic in Fig. 15.

Table 4 Effective slurry pressure conversion rates

	S0C2	S0C3	S2C2	S4C2	S6C1	S8C1	S10C1	S14C1
η/%	97.45	—	97.16	96.67	97.01	96.87	96.96	97.25

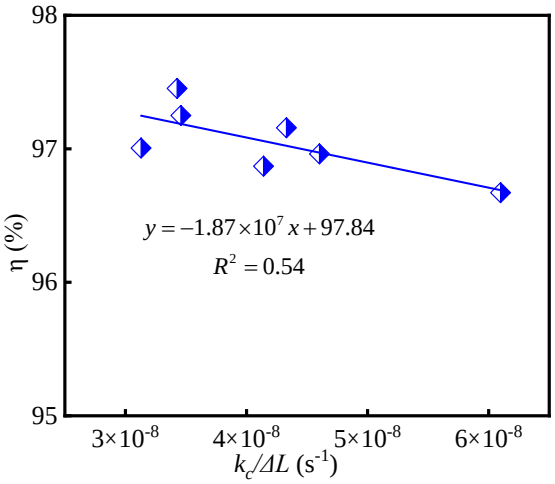

Fig. 16 Relationship between $k_c/\Delta L$ and η

4.4 Support efficiency of filter cake

The effective slurry pressure conversion rate (η) was proposed to describe the effective slurry pressure formation process and the support efficiency of filter cake (Min, 2012). Under the same support pressure, a larger η indicates that a higher effective support pressure the excavation face obtains. The η can be calculated in Eq. (2)

$$\eta = \frac{P_s - P_w - u}{P_s - P_w} \tag{2}$$

Where P_s denotes the slurry pressure; P_w denotes the hydrostatic pressure on the excavation face; and u denotes the excess pore pressure on the excavation face.

As depicted in Fig. 13, the slurry pressure used to balance the excess pore pressure is converted into effective slurry pressure during the process of excess pore pressure dissipation. As a result, the η increases and tends to stable gradually. As shown in Table 4, the effective slurry pressure conversion rate of the external filter cakes is all over 96%. The main reason is that the permeability coefficient of filter cakes is maintained at the level of 10^{-8} cm/s, which prevents the water infiltration and the increase in excess pore pressure. As a result, the external filter cakes obtain good efficiency in transforming slurry pressure to effective slurry pressure. Note that the hydraulic gradient in field situations is much lower than that in laboratory tests during SI, the filter cake is formed relatively slower and excess pore water pressure is higher in real tunnels (Xu and Bezuijen 2018, 2019), leading to a relatively larger support pressure to stabilize the tunnel face in field situations (Bezuijen *et al.* 2006). Hence, the difference of hydraulic gradient between laboratory tests and practical application should be taken into consideration during the practical application.

The relationship between $k_c/\Delta L$ and η is shown in Fig. 16. A gentle decreasing trend of η is shown with the increase of $k_c/\Delta L$, indicating that the filter cake with lower permeability coefficients and higher thicknesses obtains higher effective slurry support under the same support condition. Hence, the k_c and thickness of filter cake should be considered during the chamber opening process. According to Figs. 9 and 11, even though the water discharge can be reduced by mixing with silty sand excavated from tunnel face during FCF, the k_c of filter cake will increase at the same time, which contributes to the decrease of η. Therefore, before chamber opening, the disturbance of strata should be considered to prevent the slurry from being mixed with too much silty sand. If necessary, replacement of some sand-bentonite slurry with pure slurry can also be taken to form suitable filter cake before chamber opening. Meanwhile, η can also be increased by extending the time of SI to form a thicker filter cake.

5. Discussion

5.1 SI and the FCF process

Fig. 17 shows the SI and the FCF process. Generally, an infiltration zone and an external filter cake will form during SI and FCF in sand strata (Min *et al.* 2015). At the beginning of the SI, the pressurized slurry infiltrate into the strata (see Fig. 17(a)), small slurry particles block the strata pores, but the large particles accumulate on the surface (Sherard *et al.* 1984). As a result, an infiltration zone (mud spurt) appears first, and then the primary filter cake appears when the strata pore meets a certain criterion (Min *et al.* 2013) (see Fig. 17(b)). After that, the water in slurry will

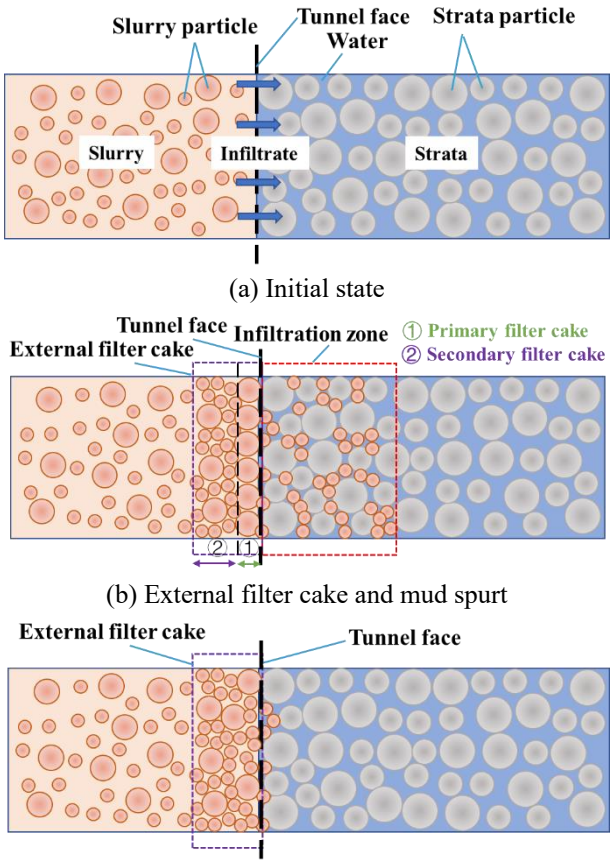

Fig. 17 Schematic layout of SI and FCF process

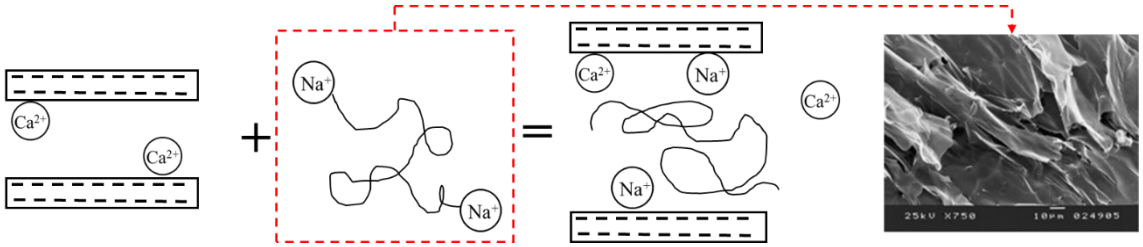

Fig. 18 SEM image and polymer intercalation process

pass through the primary filter cake and the slurry particles will deposit on it to accumulate the formation of the secondary filter cake (Lin *et al*. 2021). However, considering that pressurized slurry particles fail to infiltrate into the silty sand strata in xinjizhou shoal, only external filter cake forms on the tunnel face (see Fig. 17(c)). The silty sand whose particles are larger than that of bentonite will deposited more rapidly on the excavation face to clog the pores during this process.

5.2 Modification mechanism of CMC

Considering the excellent effect of CMC on water discharge reduction during SI and FCF, it is necessary to discuss the influence of silty sand and the modification mechanism of CMC. The CMC molecular chain was found to perform a space network structure based on the SEM (Scanning Electron Microscope) images (see Fig. 18) (Braga *et al*. 2008), and the CMC modified bentonite is essentially a typical polymer/lamellar silicate composite material (Tien and Wei 2001). During slurry modification, the polymer solution is mixed with layered silicate. Then, the layered silicate is exfoliated into nanoscale lamellar in the polymer matrix under the mechanochemical or thermodynamic influence. At the same time, with interaction between the exchangeable metal cations on the surface of slurry particles and the Na^+ ionized from CMC, the montmorillonite (a kind of lamellar silicate, the main component of bentonite) layers spacing increases to allow the intercalation of polymer molecular chain (Stutzmann and Siffert 1977). In this process, the aggregation of the montmorillonite layers will decrease obviously. According to Ray and Bousmina (2005), the polymer intercalation process can be summarized in a schematic diagram in Fig. 18.

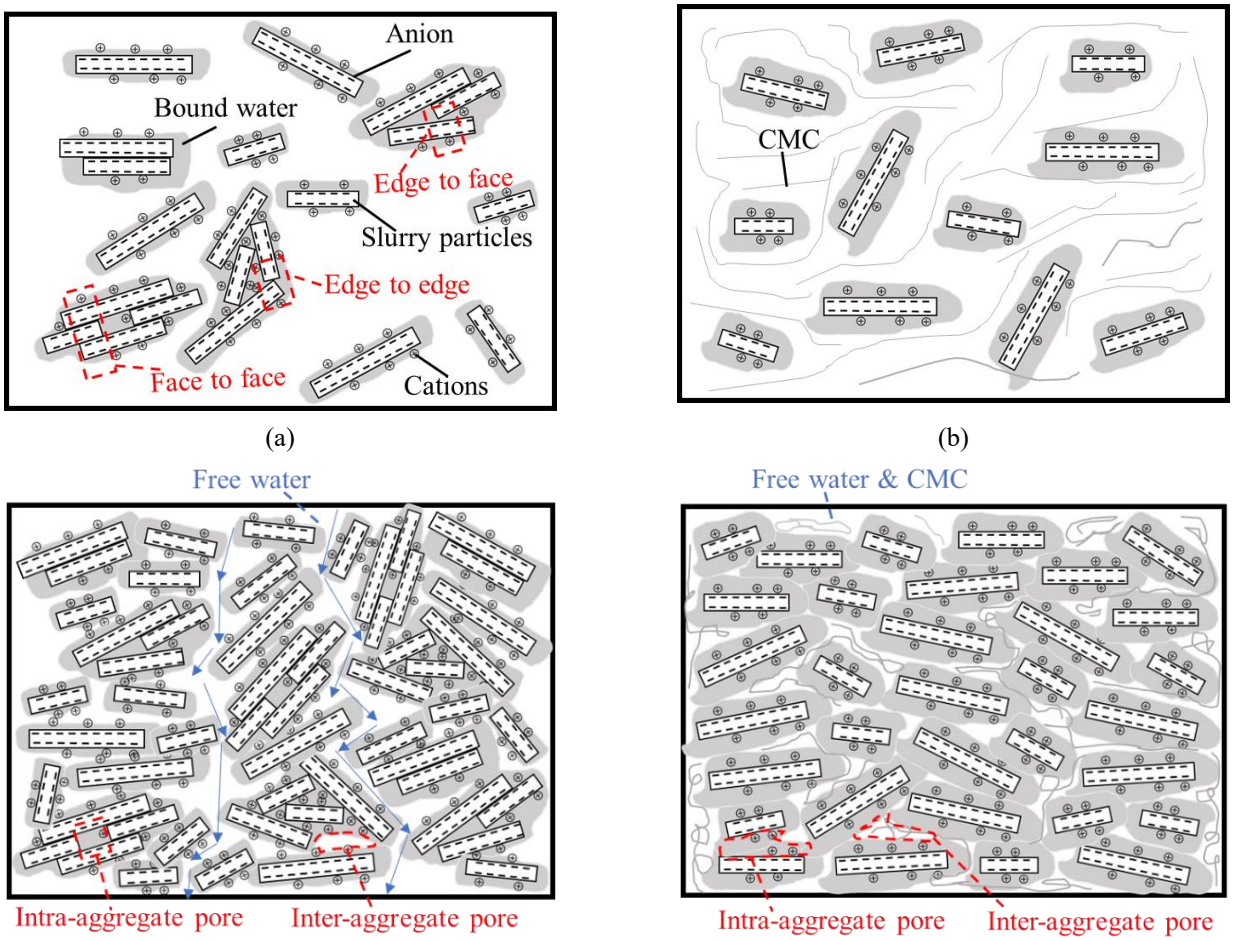

Fig. 19 Modification mechanism of CMC: (a) schematic layout of distribution of slurry particles in pure slurry, (b) schematic layout of distribution of slurry particles in CMC modified slurry, (c) schematic layout of filter cake structure before modification and (d) schematic layout of filter cake structure after modification

Most of the Na-bentonite is modified from Ca-bentonite, resulting in a few Ca-bentonite exist in Na-bentonite. The bentonite is negatively charged after being mixed with water, the Ca^{2+} adsorbed on the surface of slurry particles may neutralize more negative charges, leading to the reduction of repulsive forces between slurry particles (Zhang *et al*. 2016, Liu *et al*. 2018, Wei *et al*. 2020). As a result, the montmorillonite particles flocculate into aggregates, which can be categorized into three contact forms: Face-Face, Edge-Edge and Edge-Face (see Fig. 19(a)), respectively (Min *et al*. 2019). The agglomeration of the aggregates weakens the physical stability and homogeneity. In contrast (see Fig. 19(b)), the interlayer cations (Ca^{2+}) of bentonite react with Na^{+} ionized from CMC once the slurry encounters with the CMC. Consequently, the electrical repulsion between slurry particles increases obviously. In addition, the CMC molecular chains are dispersed in the slurry uniformly, which significantly improves the physical stability of the slurry. The viscosity of slurry, the thickness of the surface binding water and the interlayer binding water of bentonite increase accordingly (Wei *et al*. 2020).

The filter cake is considered as saturated soil full of slurry particles, bound water and free water. The pores in the filter cake can be divided into inter-aggregate pore and intra-aggregate pore (Lloret *et al*. 2003). The pore structure, which is affected by the physical arrangement and the interactive forces between the slurry particles, has some associations with the permeability of filter cake. When the bentonite is mixed with the water, some free water molecules are attracted to form bound water on the particle surface (Wang *et al*. 2018). The bound water remains stable around the slurry particles during SI and FCF. As a result, the free water only flows through the effective pores between bound water membranes (Dixon *et al*. 1985). However, the Ca^{2+} adsorbed on the surface of slurry particles reduces the number of adsorbed free water molecules, resulting in relatively thinner bound water membrane and more aggregates. Under the slurry pressure, the aggregated particles are tightly stacked to form the filter cake. The filter cake pores are mainly inter-aggregate pores with high connectivity, which makes the water pass through the effective pores in the filter cake smoothly (see Fig. 19(c)).

When the bentonite is modified by CMC, the thickness of bound water membranes and the dispersibility of

particles increase accordingly, leading to the increase of the space be occupied by water in the filter cake (see Fig. 19(d)). The intra-aggregate pore, which encompassed more bound water (Wu *et al*. 2017), is the main pores of CMC modified slurry filter cake. The existence of intra- aggregate pore blocks part of water path and decreases the permeability of filter cake. Furthermore, the CMC molecules chain, gradually bond around the bentonite molecules and build connection with slurry particles, which contributes to preventing water through the inter-aggregate pore and reducing the water discharge further.

6. Conclusions

Based on a slurry shield construction project in silty sand strata, a series of ICTs were performed to investigate the infiltration characteristics of modified slurry and the support efficiency of filter cake. The water discharge, the permeability coefficient and effective slurry pressure conversion rate of filter cake were analyzed. The SI and FCF process and the modification mechanism of CMC was clarified. The following conclusions can be drawn:

- The growth of water discharge of all the slurries becomes stable at the pressure of 300 kPa. Only external filter cake is formed in the silty sand strata of Xinjizhou shoal.
- The thickness of bound water membrane increases to block more water path in filter cake after being modified by CMC, as well as the CMC molecules chain bonds around the bentonite molecules to prevent water from passing through the inter-aggregate pore. It is proved that only one thousandth of a percent increment of CMC reduces the water discharge with 15%.
- Although the silty sand excavated from the tunnel face benefits to the reduction of water discharge. The uniformity of the filter cake gets worse obviously with increasing silty sand content. The filter cake surface sag can be observed after the silty sand content exceeds 10%, which may pose a threat to the chamber opening under compressed air pressure. Therefore, it is necessary to keep silty sand content within 10%.
- The k_c of the external filter cakes ranges from 3.83×10^{-8} cm/s to 7.44×10^{-8} cm/s. The effective slurry pressure conversion rate of the external filter cakes is all beyond 96%, which decrease with increasing $k_c/\Delta L$.

Acknowledgements

This study is partially supported by the National Natural Science Foundation of China (Grant No. 51978159), National Key R&D Program of China (Grant No. 2015BAB07B06).

References

Anagnostou, G. and Kovári, K. (1994), "The face stability of slurry-shield-driven tunnels", *Tunn. Undergr. Sp. Tech*., **9**(2), 165–174. https://doi.org/10.1016/0886-7798(94)90028-0.

ASTM (American Society for Testing and Materials) (2006), Standard test method for permeability of granular soils (constant head). ASTM D2434-06. ASTM, West Conshohocken, PA, USA.

ASTM (American Society for Testing and Materials) (2007), Standard test method for particle-size analysis of soils. ASTM D422, West Conshohocken, PA, USA.

Aydin, A., Ozbek, A. and Cobanoglu, I. (2004), "Tunnelling in difficult ground: a case study from dranaz tunnel, sinop, turkey", *Eng. Geol.*, **74**(3), 293-301. https://doi.org/10.1016/j.enggeo.2004.04.003.

Bezuijen, A., Pruiksma, J.P. and van Meerten, H.H. (2006), *Pore Pressures in front of Tunnel, Measurements, Calculations and Consequences for Stability of Tunnel Face. In Tunnelling. A Decade of Progress. GeoDelft 1995–2005* (Eds., A. Bezuijen and H. van Lottum), 35-41. Leiden, the Netherlands: Taylor & Francis (Balkema).

Braga, M., Pato, M., Silva, H., Ferreira, E.I., Gil, M.H. and Duarte, C. (2008), "Supercritical solvent impregnation of ophthalmic drugs on chitosan derivatives", *J. Supercritical Fluid.*, **44**(2), 245-257. https://doi.org/10.1016/j.supflu.2007.10.002.

Broere, W. (2001), "Tunnel face stability & new CPT application", PhD Dissertation. Delft University of Technology, Delft, Netherlands.

Broere, W. (2016), "Urban underground space: solving the problems of today's cities", *Tunn. Undergr. Sp. Tech*., **55**, 245-248. https://doi.org/10.1016/j.tust.2015.11.012.

Duong, T.V., Trinh, V.N., Cui, Y.J., Tang, A.M. and Calon, N. (2013), "Development of a large-scale infiltration column for studying the permeability of unsaturated fouled ballast", *Geotech. Test. J.*, 36, 1-10. https://doi.org/10.1520/GTJ20120099.

Dixon, D.A., Gray, M.N. and Thomas, A.W. (1985), "A study of the compaction properties of potential clay-sand buffer mixtures for use in nuclear fuel waste disposal", *Eng. Geol*., **21**, 247-255. https://doi.org/10.1016/0013-7952(85)90015-8.

Fritz, P., Stengele, R.H. and Heinz, A. (2002), "Modified bentonite slurries for slurry shields in highly permeable soils", *Proceedings of the 4rth International Symposium Geotechnical Aspects of Underground Construction in Soft Ground*, Toulouse, France.

Fritz, P. (2007), "Additives for slurry shields in highly permeable ground", *Rock Mech. Rock Eng.*, **40**(1), 81-95. https://doi.org/10.1007/s00603-006-0090-y.

Hu, X.Y. and Zhang, Z.X. (2009), "Analysis of effect of slurry infiltration on shear strength of soil of excavation face in slurry shield under general stress condition", *Chinese J. Rock Mech. Eng*., **28**(5), 1027-1036. (In Chinese).

Lee, I.M., Nam, S.W. and Ahn, J.H. (2003), "Effect of seepage forces on tunnel face stability", *Can. Geotech. J.*, **40**(2), 342-350. https://doi.org/10.1139/t02-120.

Li, X. and Yuan, D. (2018), "Creating a working space for modifying and maintaining the cutterhead of a large-diameter slurry shield: a case study of Beijing railway tunnel construction", *Tunn. Undergr. Sp. Tech.*, **72**, 73-83. https://doi.org/10.1016/j.tust.2017.11.008.

Lin, C.G., Zhang, Z.M., Wu, S.M. and Yu, F. (2013), "Key techniques and important issues for slurry shield under-passing embankments: a case study of Hangzhou Qiantang river tunnel", *Tunn. Undergr. Sp. Tech.*, **38**(9), 306-325. https://doi.org/10.1016/j.tust.2013.07.004.

Lin, Y., Fang, Y., He, C. and Wang, W. (2021), "Experimental study on degree of match between slurry and ground based on particle retention rate", *Tunn. Undergr. Sp. Tech.*, https://doi.org/10.1016/j.tust.2021.104105.

Liu, P.F., Wang, S.Y., Ge, L., Thewes, M., Yang, J.S. and Xia, Y.M. (2018), "Changes of atterberg limits and electrochemical

behaviors of clays with dispersants as conditioning agents for EPB shield tunnelling", *Tunn. Undergr. Sp. Tech.*, **73**, 244-251. https://doi.org/10.1016/j.tust.2017.12.026.

Lloret, A., Villar, M.V., Sa'nchez, M., Gens, A., Pintado, X. and Alonso, E.E. (2003). "Mechanical behaviour of heavily compacted bentonite under high suction changes", *Géotechnique*, **53**(1), 27-40. https://doi.org/10.1680/geot.53.1.27.37258.

Mao, J., Yuan, D., Jin, D., Wang, B. and Wu, S. (2021), "Experimental study on electrical resistivity characteristics of saturated sand mixes with bentonite slurry", *Appl. Sci.*, **11**, 12126. https://doi.org/10.3390/app112412126.

Min, F.L. (2012), "Laws of slurry infiltration in soils and filter cake formation in slurry type shield", PhD Dissertation, college of environment, HoHai University, Nanjing, P.R. China (in Chinese).

Min, F.L., Zhu，W. and Han, X.R. (2013), "Filter cake formation for slurry shield tunneling in highly permeable sand", *Tunn. Undergr. Sp. Tech.*, **38**, 423-430. https://doi.org/10.1016/j.tust.2013.07.024.

Min, F.L., Zhu，W., Lin, C. and Guo, X. (2015), "Opening the excavation chamber of the large-diameter size slurry shield: a case study in Nanjing Yangtze river tunnel in China", *Tunn. Undergr. Sp. Tech.*, **46**, 18-27. https://doi.org/10.1016/j.tust.2014.10.002.

Min, F.L., Song, H. and Zhang, N. (2018), "Experimental study on fluid properties of slurry and its influence on slurry infiltration in sand stratum", *Appl, Clay Sci,*, **161**, 64-69. https://doi.org/10.1016/j.clay.2018.03.028.

Min, F.L., Du, J.R. and Zhang, N. (2019), "Experimental study on property change of slurry and filter cake of slurry shield under seawater intrusion", *Tunn. Undergr. Sp. Tech.*, **88**, 290-299. https://doi.org/10.1016/j.tust.2019.03.006.

Ni, L.A., Yu, A.B., Lu, G.Q. and Howes, T. (2006), "Simulation of the cake formation and growth in cake filtration", *Miner. Eng.*, **19**(10), 1084-1097. https://doi.org/10.1016/j.mineng.2006.03.012.

Park, J.K. (2022), "Reliability analysis of tunnel face stability considering seepage effects and strength conditions", *Geomech. Eng.*, **29**(3), 331-338. https://doi.org/10.12989/gae.2022.29.3.331.

Ray, S.S. and Bousmina, M. (2005), "Biodegradable polymers and their layered silicate nanocomposites: In greening the 21st century materials world", *Progress Mater. Sci.*, **50**(8), 962-1079. https://doi.org/10.1016/j.pmatsci.2005.05.002.

Sherard, J.L., Dunnigan, L.P. and Talbot, J.R. (1984), "Basic properties of sand and gravel filters", *J. Geotech. Eng.*, **110**(6), 684-700. https://doi.org/10.1061/(ASCE)0733-9410(1984)110:6(684).

Stutzmann, T. and Siffert, B. (1977), "Contribution to the adsorption mechanism of acetamide and polyacrylamide on to clays". *Clays Clay Miner.*, **25**(6), 392-406. https://doi.org/10.1346/CCMN.1977.0250604.

Tien, Y.I.. and Wei, K.H. (2001), "Hydrogen bonding and mechanical properties in segmented montmorillonite/polyurethane nanocomposites of different hard segment ratios", *Polymer*, **42**(7), 3213-3221. https://doi.org/10.1016/S0032-3861(00)00729-1.

Talmon, A.M., Mastbergen, D.R. and Huisman, M. (2013), "Invasion of pressurized clay suspensions into granular soil", J. *Porous Media*, **16**, 351-365. https://doi:10.1615/JPorMedia.v16.i4.70.

Wang, S.W., Zhu, W., Fei, K., Xu, C.Y. and Zhang, N. (2018), "Study on non-darcian flow sand clay mixtures", *Appl. Clay Sci*., **151**, 102-108. https://doi.org/10.1016/j.clay.2017.10.028.

Wei, C., Liu, D., Song H.F., Zhang, S.R. and He, S.W. (2020), "Experimental study of salt-resisting slurry for undersea shield tunnelling", *Tunn. Undergr. Sp. Tech.*, **98**, 103322. https://doi.org/10.1016/j.tust.2020.103322.

Wu, T., Wang, Z., Wang, H., Zhang, Z. and Van Loon, L.R. (2017), "Salt effects on Re(VII) and Se(IV) diffusion in bentonite". *Appl. Clay Sci.*, **141**, 104-110. https://doi.org/10.1016/j.clay.2017.02.021.

Xu, T. and Bezuijen, A. (2018), "Bentonite slurry infiltration into sand, filter cake formation under various conditions", *Géotechnique*, **69**(12), 1095-1106. https://doi.org/10.1680/jgeot.18.P.094.

Xu, T. and Bezuijen, A. (2019), "Experimental study on the mechanisms of bentonite slurry penetration in front of a slurry TBM", *Tunn. Undergr. Sp. Tech.*, **93**, 1-10. https://doi.org/10.1016/j.tust.2019.103052.

Zhang, L., Sun, D. and Jia, D. (2016), "Shear strength of GMZ07 bentonite and its mixture with sand saturated with saline solution", *Appl. Clay Sci.*, **132-133**, 24-32. https://doi.org/10.1016/j.clay.2016.08.004.

Zhang, N., Yu, X.B., Pradhan, A. and Puppala, A.J. (2017), "A new generalized soil thermal conductivity model for sand–kaolin clay mixtures using thermo-time domain reflectometry probe test", *Acta Geotechnica*, **12**(4), 739-752. https://doi.org/10.1007/s11440-016-0506-0.

Zhao, J., Gong, Q.M. and Eisensten, Z. (2007), "Tunnelling through a frequently changing and mixed ground: a case history in Singapore", *Tunn. Undergr. Sp. Tech.*, **22**(4), 388-400. https://doi.org/10.1016/j.tust.2006.10.002.

Zizka, Z., Schoesser, B., Thewes, M. and Schanz, T. (2018), "Slurry shield tunneling: new methodology for simplified prediction of increased pore pressures resulting from slurry infiltration at the tunnel face under cyclic excavation processes", *Inte. J. Civil Eng*., **15**(4), 387-405. https://doi.org/10.1007/s40999-018-0303-2.

Zizka, Z. and Thewes, M. (2016), *Recommendations for Face Support Pressure Calculations for Shield Tunnelling in Soft Ground.* In Deutscher Ausschuss für unterirdisches Bauen e. V. (DAUB) - German Tunnelling Committee (ITA-AITES).

Zizka, Z., Schoesser, B. and Thewes, M. (2021), "Investigations on the transient support pressure transfer at the tunnel face during slurry shield drive Part 2: Case B – Deep slurry penetration exceeds tool cutting depth", *Tunn. Undergr. Sp. Tech.*, **118**, 104196. https://doi.org/10.1016/j.tust.2021.104169.

Zhang, N., Yu, X.B., Pradhan, A. and Puppala, A.J. (2017), "A new generalized soil thermal conductivity model for sand–kaolin clay mixtures using thermo-time domain reflectometry probe test", *Acta Geotechnica*, **12**(4), 739-752. https://doi.org/10.1007/s11440-016-0506-0.

Zou J.F., Wei. A. and Liang L. (2020), "Analytical solution for steady seepage and groundwater inflow into an underwater tunnel", *Geomech. Eng*., **20**(3), 367-273. https://doi.org/10.12989/gae.2020.20.3.267.

CC